Spin-Orbit Coupling and Spin Textures in Optical Superlattices

Junru Li, Wujie Huang, Boris Shteynas, Sean Burchesky, Furkan Çağrı Top, Edward Su, Jeongwon Lee, Alan O. Jamison, and Wolfgang Ketterle

Research Laboratory of Electronics, MIT-Harvard Center for Ultracold Atoms, Department of Physics, Massachusetts Institute of Technology, Cambridge, Massachusetts 02139, USA

(Received 10 June 2016; revised manuscript received 17 August 2016; published 27 October 2016)

We propose and demonstrate a new approach for realizing spin-orbit coupling with ultracold atoms. We use orbital levels in a double-well potential as pseudospin states. Two-photon Raman transitions between left and right wells induce spin-orbit coupling. This scheme does not require near resonant light, features adjustable interactions by shaping the double-well potential, and does not depend on special properties of the atoms. A pseudospinor Bose-Einstein condensate spontaneously acquires an antiferromagnetic pseudospin texture, which breaks the lattice symmetry similar to a supersolid.

DOI: 10.1103/PhysRevLett.117.185301

Spin-orbit coupling is the mechanism for many intriguing phenomena, including $\mathbb{Z}_2$ topological insulators, the spin quantum Hall effect [1,2], Majorana fermions [3], and spintronics devices [4]. Realizing controllable spin-orbit coupling with ultracold atoms should make it feasible to explore fundamental aspects of topology in physics and applications in quantum computing [5].

Spin-orbit coupling requires the atom's motion to be dependent on its spin state. Spin-orbit coupling without spin flips is possible for schemes that are diagonal in the spin component σ_z. Such spin-dependent vector potentials, which are sufficient for realizing quantum spin Hall physics and topological insulators, can be engineered using far-detuned laser beams to completely suppress spontaneous emission [6,7].

However, spin flips (i.e., spin-orbit coupling terms involving σ_x or σ_y operators) are necessary for Rashba [8] and Dresselhaus [9] spin-orbit coupling [10]. Experiments with ultracold atoms couple pseudospin states using optical dipole transitions, which couple only to the orbital angular momentum of the atom. Most realizations, including the first demonstration [11], use hyperfine states of an alkali atom as pseudospins. In this case, the coupling of the two states occurs due to internal spin-orbit coupling in the excited state of the atom, which causes the fine-structure splitting between the D_1 and D_2 lines. The optimum detuning of the lasers is comparable to this splitting, leading to heating. Special atomic species with orbital angular momentum in the ground state can avoid this problem, as recently realized with dysprosium [12]. Here, we present a new method that can be applied to any atomic species, using an external orbital degree of freedom as the pseudospin to avoid the need for near-resonant light.

An external degree of freedom as the pseudospin could be realized for a two-dimensional system by using the ground and first excited states of the confinement along the third dimension as pseudospin states. However, the excited state would rapidly relax due to elastic collisions, typically on a millisecond time scale [13]. This is also the case for the recent implementation of spin-orbit coupling (SOC) with hybrid s-p Floquet bands in a one-dimensional optical lattice [14]. To solve this issue, we choose an asymmetric double-well potential (Fig. 1). Pseudospins up and down are realized as the two lowest eigenstates of the double-well potential. For $J/\Delta \ll 1$, they can be expressed by the tight-binding states $|l\rangle$ and $|r\rangle$ localized in the left and right wells, respectively: $|\downarrow\rangle = |l\rangle + (J/\Delta)|r\rangle$ and

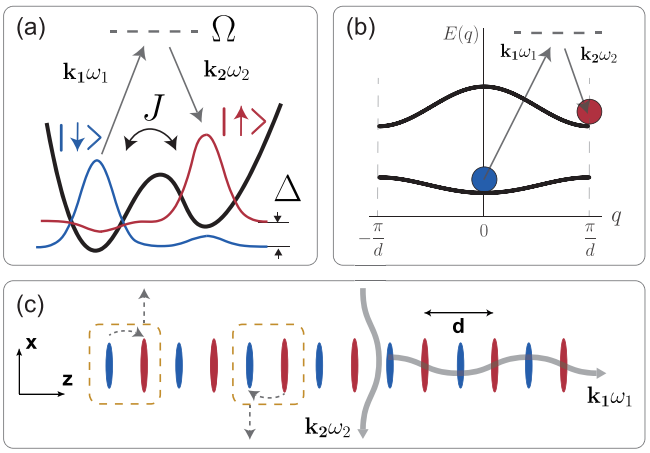

FIG. 1. Realization of orbital pseudospins in a superlattice. (a) The unit cell of the superlattice is a double well with offset Δ and tunneling J. The two lowest eigenstates (pseudospin up and down) are coupled via a two-photon Raman process. (b) Raman process in the band structure of the superlattice. The ground state with quasimomentum $q = 0$ is coupled to the edge of the Brillouin zone $q = (\pi/d)$ of the first excited band. (c) Top view of the superlattice with period $d = \lambda_{\mathrm{IR}}/2 = 532$ nm. Raman coupling is implemented by two λ_{IR} beams: one along the superlattice (z direction), the other along the x direction. SOC (curved arrows) transfers transverse recoil in the x direction to the atoms (dashed arrows).

$|\uparrow\rangle = |r\rangle - (J/\Delta)|l\rangle$. The tunneling J and offset Δ between the two wells are used to adjust the overlap—and therefore the interactions and the collisional relaxation rate—between the two pseudospin states. We couple the two states via a two-photon Raman transition with large detunings to achieve SOC with spin flips. (For convenience, we will refer to pseudospin as spin in this Letter.) Recent work on two-leg ladders can be mapped to SOC between the two legs of the ladder [15,16]. Our scheme is qualitatively different from other realizations of orbital pseudospin since it realizes spin-orbit coupling in free space as compared to lattice models.

An intriguing prediction for spin-orbit coupled Bose-Einstein condensates (BECs) is the existence of a stripe phase [17–19], a spontaneous density modulation that realizes a supersolid [20]. However, when the interspin ($g_{\uparrow\downarrow}$) and intraspin ($g_{\uparrow\uparrow}$, $g_{\downarrow\downarrow}$) interaction strengths are the same, the increased interaction energy of the density modulation drives spatial phase separation, eliminating the stripes. The system can be kept in the miscible phase when interspin interactions are weaker than intraspin interactions, $g_{\uparrow\downarrow}^2 < g_{\uparrow\uparrow} g_{\downarrow\downarrow}$ [19]. In our realization, $g_{\uparrow\downarrow}$ is proportional to the overlap squared of the wave functions on the two sides of the double well. An analogous scheme can be realized with hyperfine pseudospins and spin-dependent lattices [21], but requires near-resonant light. Our scheme does not depend on specific atomic properties and addresses three challenges to realizing the stripe phase: (1) spin-orbit coupling without near resonant light, (2) a miscible system with adjustable interspin interactions, (3) a long lifetime against collisional relaxation.

Instead of one double-well system, we create a lattice of double wells using an optical superlattice [Fig. 1(c)]. The advantages of working with a stack of coherently coupled double wells are twofold: the increased signal to noise ratio and the use of interference between the double wells to separately observe the two spin states. In the present work, the degree of freedom along the superlattice direction is purely an aid to observation [22].

Our main result is the observation of the momentum structure of a BEC modified by a superlattice and spin-orbit coupling. We first describe the effects of the superlattice without adding SOC. A one-dimensional superlattice of double wells was realized by combining lattices of $\lambda_{\mathrm{IR}} =$ 1064 nm light and $\lambda_{\mathrm{Gr}} = 532$ nm light obtained by frequency doubling the $\lambda_{\mathrm{IR}} = 1064$ nm light. The shape of the double-well unit cell is determined by the relative strength and spatial phase ϕ_{SL} between the two lattices. The phase is controlled by a rotatable dispersive glass plate and an acousto-optical modulator for rapidly switching the IR lattice frequency.

The experiment starts with a BEC of $\sim 3 \times 10^5$ ^{23}Na atoms in the $|F = 1, m_F = -1\rangle$ state in a crossed optical dipole trap. The superlattice is adiabatically ramped up within 250 ms. For an offset $\Delta \gg J$, all the atoms

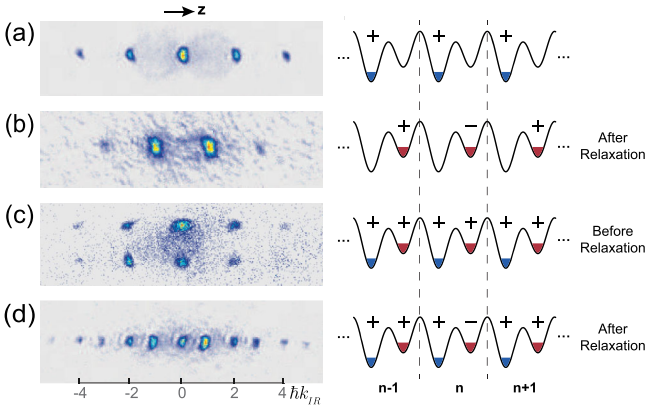

FIG. 2. Spontaneous formation of an antiferromagnetic spin texture. (a),(b) Time-of-flight (TOF) pattern of atoms in the ground (first excited) band of the superlattice. After preparation of the $|\uparrow\rangle$ state with quasimomentum $q = 0$, it relaxes to the bottom of the band at $q = \pi/d$. (c) An equal mixture of spin states is prepared by rapidly switching the superlattice parameters. The two spin states can be separated in the TOF by a pseudospin Stern-Gerlach effect [23]. The figure shows that both spin states are in $q = 0$ before the relaxation. (d) After relaxation, spinor BECs with states $|\downarrow\rangle$, $q = 0$ and $|\uparrow\rangle$, $q = \pi/d$ are observed. The momentum pattern implies a periodic structure at $2d$, twice the lattice constant, indicating that an antiferromagnetic spin structure with a doubled unit cell has formed. The plus and minus signs indicate (one possible choice for) the phase of the BEC wave function. n is the site index.

equilibrate at the band minimum $q = 0$ of the lowest superlattice band, putting 100% of the population in the $|\downarrow\rangle$ state. The relative population of the two spin states can be controlled by first adjusting Δ for the loading stage to achieve a desired state population and then rapidly lifting one well up to the final offset [23]. The upper well corresponds to the first excited band, which has its minimum energy at quasimomentum $q = \pi/d$ with $d = \lambda_{\mathrm{IR}}/2$ [Figs. 2(a) and 2(b)]. Since the lowest energy $|\uparrow\rangle$ and $|\downarrow\rangle$ states have different quasimomenta and experience different transverse confinement, they can be separately observed in ballistic expansion images without the band-mapping techniques [23].

The π/d quasimomentum difference also leads to an interesting spin texture for an equal population of the $|\uparrow\rangle$ and $|\downarrow\rangle$ states. For this, atoms are prepared in both bands with $q = 0$ [Fig. 2(c)], corresponding to a wave function periodicity of 532 nm, i.e., the lattice constant. However, after relaxation, the periodicity has doubled to 1064 nm, as indicated by the doubled number of momentum components in ballistic expansion images [Fig. 2(d)]. Specifically, the system was prepared in the symmetric state $\sum_n(|\downarrow_{\mathrm{n}}\rangle + |\uparrow_{\mathrm{n}}\rangle)$, where n denotes the lattice site, which is a ferromagnetic spin state in the x-y plane. After relaxation into the state $\sum_n[|\downarrow_{\mathrm{n}}\rangle + (-1)^n e^{i\theta} e^{-i\Delta t}|\uparrow_{\mathrm{n}}\rangle]$ an antiferromagnetic spin texture has developed, which reduces the translational symmetry of the lattice. This

TABLE I. The amplitudes of the wave functions in Eqs. (1) and (2) obtained from first order perturbation theory ($i = 1, 2$).

States	M_i	M_i'	K
$\|\Psi_1\rangle$	$-\frac{1}{2}(\Omega/E_r - \delta)$	$-\frac{1}{2}(\Omega/E_r + \delta)$	$-i[e^{-i(\pi/4)}/\sqrt{2}](J/\Delta)(\Omega/E_r + \Delta - \delta)$
$\|\Psi_2\rangle$	$+\frac{1}{2}(\Omega/E_r + \delta)$	$-\frac{1}{2}(\Omega/E_r - \delta)$	$+i[e^{i(\pi/4)}/\sqrt{2}](J/\Delta)(\Omega/E_r - \Delta + \delta)$

system breaks both U(1) symmetry (the phase of the BEC) and the translational symmetry of the superlattice. In addition to the spin-density wave, it also has a density wave with the same period due to the interference of the $|\uparrow\rangle$ and $|\downarrow\rangle$ satellites. The position of the spin and density modulations is determined by the spontaneous phase θ and oscillates at frequency Δ [23]. It is a simple system fulfilling one definition of supersolidity [25–27].

The small satellites allow spin-orbit coupling, but also lead to the collisional decay of the $|\uparrow>$ state. We observed lifetimes on the order of 200 ms for both the $|\uparrow\rangle$ and equally mixed states at a density of $n \approx 2.5 \times 10^{14}$ cm^{-3}. The similar lifetimes for both states and the sensitivity to daily alignment indicate the lifetime being limited by technical noise and the misalignment of the lattice rather than by collisions. Collisions would lead to a shorter lifetime for the mixed state by a factor of $4(J/\Delta)^2$. Adding Raman beams (with the parameters presented in Fig. 4) increases the loss rate by $\sim$10/s, probably caused by technical issues. While previous work with ^{87}Rb reports a lifetime of seconds [11], the Raman hyperfine spin flip scheme is not promising for lighter atoms because of the substantially higher heating rates compared with ^{87}Rb, which are 10^3 (10^5) times higher for ^{23}Na (^{6}Li) [28]. Even without major improvements, the lifetimes achieved in our work are longer than any relevant dynamic time scale and should be sufficient for further studies, including the observation of the stripe phase [29].

Coupling between the two spin states is provided by two λ_{IR} beams: one along the superlattice direction z, the other orthogonal to it (along x). The frequency difference of the two beams is close to the offset in the double well, allowing near-resonant population transfer. The recoil k_z along the lattice is necessary to couple the two orthogonal spin states in the double well, and was chosen to be $k_z = \pi/d$. The recoil kick k_x in the transverse plane provides the coupling between the free-space motion in the transverse plane and the spin. It has opposite signs for the transition $|\downarrow\rangle$ to $|\uparrow\rangle$ and the reverse transition.

The Raman coupling can be described as a moving potential $V_{\mathrm{Raman}} = \Omega\cos(k_x x + k_z z - \delta t)$, characterized by a two-photon Rabi frequency Ω, a detuning of Raman beams δ, and a wave vector $(k_x, 0, k_z)$. We characterize the states by their spin, quasimomentum q, and x momentum k_x (the y momentum is always zero).

If the system is initially prepared in the state $|\downarrow, q = 0, k_x = 0\rangle$, the adiabatically ramped Raman beams will transfer it to a new eigenstate:

$$|\Psi_1\rangle = |\downarrow, 0, 0\rangle + K_1 e^{-i\delta t}|\uparrow, \pi/d, k_x\rangle + M_1 e^{-i\delta t}|\downarrow, \pi/d, k_x\rangle + M_1{}' e^{i\delta t}|\downarrow, -\pi/d, -k_x\rangle. \quad (1)$$

If prepared in $|\uparrow, \pi/d, 0\rangle$, the new state will be

$$|\Psi_2\rangle = e^{-i\Delta t}|\uparrow, \pi/d, 0\rangle + K_2 e^{i(\delta-\Delta)t}|\downarrow, 0, -k_x\rangle + M_2 e^{i(\delta-\Delta)t}|\uparrow, 0, -k_x\rangle + M_2{}' e^{-i(\delta+\Delta)t}|\uparrow, 0, k_x\rangle. \quad (2)$$

The amplitudes obtained from first order perturbation theory appear in Table I. The spin-orbit coupling is described by the second term in Eqs. (1) and (2). In addition, the Raman beams act as a comoving lattice and (in the limit $\delta \gg E_r$) create a moving density modulation in the two spin states, described by the third and fourth terms. The spin-orbit coupling shows a resonant behavior for $\delta \approx \Delta$—the range of interest for SOC—where the moving density modulation is nonresonant. Both contributions are proportional to Ω/Δ. The off-resonant counterrotating spin flip term is proportional to Δ^{-2} and has been neglected. For $\delta \gg E_r$, all off-resonant amplitudes M_i, M_i' become $\approx\Omega/\delta$. For $\delta = \Delta$ and both spin states populated, the spin-orbit admixture of $|\Psi_1\rangle$ is expected to form a stationary interference pattern with $|\Psi_2\rangle$ along x with wave vector k_x, and vice versa, which constitutes the stripe phase of spin-orbit coupled BECs in the perturbative limit. (In general, the periodicity of the stripes depends on β and the atoms' interactions [19].)

The resonant Raman coupling leads to the standard spin-orbit Hamiltonian [23]:

$$\hat{H}_{\mathrm{SOC}} = \frac{(\hat{p} + \alpha\hat{\sigma}_z)^2}{2m} + \beta\hat{\sigma}_x + \delta_0\hat{\sigma}_z, \quad (3)$$

which can be considered as equal contributions of Rashba and Dresselhaus interactions. The parameters $\alpha = -k_x/2$, $\beta = (1/\sqrt{2})\Omega J/\Delta$, and $\delta_0 = (\delta - \Delta)/2$ are independently tunable in our experiment.

To characterize all the components of the wave functions above, the Raman coupling was adiabatically switched on by ramping up the intensity of the two Raman beams. The momentum space wave function was observed by suddenly switching off the lattice and trapping beams and measuring the resulting density distribution with absorption imaging after 10 ms of ballistic expansion (Fig. 3).

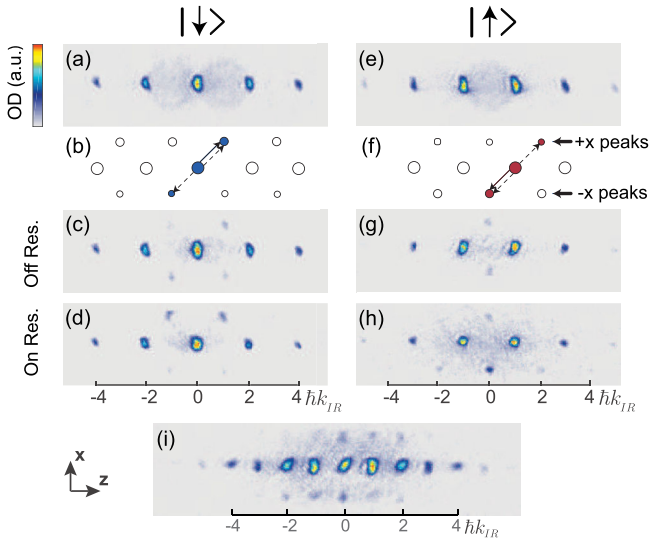

FIG. 3. Characterization of spinor BECs through their momentum distributions. (a),(e) TOF images of the $|\downarrow\rangle$ and $|\uparrow\rangle$ states, respectively. (b),(f) Schematics of the momentum peaks for $|\downarrow\rangle$ and $|\uparrow\rangle$ with Raman coupling. Both the SOC (solid arrows) and the density modulation (dashed arrows) are shown. The main peak (filled circle) is equal to the quasimomentum of the state. Extra peaks (open circles) appear due to the periodic potential. (c),(d),(g),(h) Same as in (a) and (e), but now with Raman coupling at different detunings δ. The momentum components created by the Raman process are vertically shifted compared to (a) and (e) due to the transverse momentum kick. The momentum shift along the superlattice (z direction) reflects the π/d quasimomentum of the Raman lattice. The off-resonant density modulation creates momentum peaks that are symmetric along $+x$ and $-x$ [(c) and (g)], whereas resonant spin-orbit coupling creates unidirectional momentum transfer resulting in asymmetry [(d) and (h)]. (i) Spin-orbit coupled BEC with equal population in the spin up and spin down states.

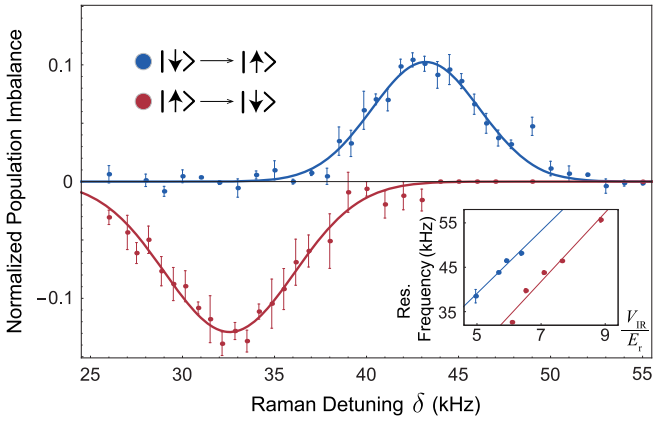

FIG. 4. Spin-orbit coupling resonances. Shown is the population imbalance between the "$+x$" and "$-x$" momentum peaks versus Raman detuning for the $|\downarrow\rangle \rightarrow |\uparrow\rangle$ (blue) and $|\uparrow\rangle \rightarrow |\downarrow\rangle$ (red) processes. The two sets of data were measured for the same superlattice parameters $V_{\mathrm{IR}} = 7.5(2)E_r$, $V_{\mathrm{Gr}} = 20(2)E_r$, and $\phi_{\mathrm{SL}} \approx 0.22(1)\pi$, which gives $\Delta \approx 37(1)$ kHz. The spin-orbit coupling strength β was calculated to be 0.40(5) kHz. The solid lines are Gaussian fits to the resonances centered at 32.2(3) and 43.2(3) kHz. The Gaussian profile of the IR lattice inhomogeneously broadens the resonances. The error bars represent 1σ statistical uncertainty. Inset: resonance center frequencies versus the IR lattice depth V_{IR} for fixed ϕ_{SL}. The resonances are linear in V_{IR} with a constant split equal to twice the recoil energy. The slope of the linear fit reveals ϕ_{SL}. The error bars are the uncertainties of the fit.

The momentum components created by the Raman beams are displaced in the x direction by the recoil shift $\hbar k_{\mathrm{IR}}$. For off-resonant Raman beams, the pattern is symmetric for the $+x$ and $-x$ directions—signifying the moving density modulation [see Eqs. (1) and (2)]. The resonant spin-orbit coupling is one sided, with opposite transfer of x momentum for the two spin states—as observed in Fig. 3. We separate the momentum peaks due to the moving density modulation from SOC by evaluating the difference between the momentum peaks along the $+x$ and $-x$ directions. Figure 4 shows the resonance feature of the SOC when the Raman detuning was varied. The resonances for the two processes $|\downarrow\rangle \rightarrow |\uparrow\rangle$ and $|\uparrow\rangle \rightarrow |\downarrow\rangle$ should be separated by $2E_r \approx 15.3$ kHz. The observed discrepancy is consistent with mean field interactions, which reduce the separation by $\sim 2\mu \approx 5$ kHz, where μ is the single site chemical potential. The observed widths of the resonances are probably dominated by the inhomogeneity of Δ due to the Gaussian beam profile of the IR lattice laser [23].

Having established spin-orbit coupling at the single-particle level, the next step is to explore the phase diagram of spin-orbit coupled Bose-Einstein condensates with interactions [17,19,21], particularly the stripe phase. The clear signature of the stripe phase is the stationary, periodic density modulation on the BEC mentioned above. The periodicity is tunable through the spin-orbit coupling strength and can be directly observed via Bragg scattering [30]. In contrast to experiments carried out with ^{87}Rb, which has similar inter- and intraspin scattering lengths, our system has an adjustable interspin interaction $g_{\downarrow\uparrow} \approx (J/\Delta)^2 g_{\downarrow\downarrow} = (J/\Delta)^2 g_{\uparrow\uparrow}$. Small values of $g_{\downarrow\uparrow}/g_{\uparrow\uparrow}$ lead to a large window of β for observing the stripe phase and enable higher contrast stripes [19]. Figure 3(i) shows the momentum distribution of an equal spin mixture with SOC. We observed an ~40 ms lifetime for the parameters presented in Fig. 4. After adding Bragg detection, the observation of the stripe phase is in reach.

In conclusion, we proposed and demonstrated a new scheme for realizing spin-orbit coupling using superlattices. An asymmetric double-well potential provides attractive features for pseudospins, including long lifetimes, adjustable interactions, and easy detection. This scheme can be applied to a wide range of atoms including lithium and potassium, which suffer from strong heating when hyperfine pseudospins are coupled. On the other hand, by

combining multiple hyperfine states with the orbital degree of the double well, our scheme can realize two-dimensional Rashba spin-orbit coupling [31] and suggestions made for alkaline-earth atoms, for example, synthetic non-Abelian gauge potentials [32,33], and Kondo lattice models [34–36].

We acknowledge helpful discussions with S. Stringari, E. Mueller, and N. Cooper. We thank A. Keshet for contributions to building the experiment and J. Amato-Grill, C. J. Kennedy, and P. N. Jepsen for suggestions and a critical reading of the manuscript. We acknowledge support from the NSF through the Center for Ultracold Atoms and by Grant No. 1506369, from Army Research Office –Multidisciplinary University Research Initiative Non-equilibrium Many-body Dynamics (Grant No. W911NF-14-1-0003), and from Air Force Office of Scientific Research – Multidisciplinary University Research Initiative Quantum Phases of Matter (Grant No. FA9550-14-1-0035).

J. L. and W. H. contributed equally to this work.

[1] M. Z. Hasan and C. L. Kane, Rev. Mod. Phys. **82**, 3045 (2010).
[2] X.-L. Qi and S.-C. Zhang, Rev. Mod. Phys. **83**, 1057 (2011).
[3] R. Wei and E. J. Mueller, Phys. Rev. A **86**, 063604 (2012).
[4] I. Žutić, J. Fabian, and S. Das Sarma, Rev. Mod. Phys. **76**, 323 (2004).
[5] J. Alicea, Y. Oreg, G. Refael, F. von Oppen, and M. P. A. Fisher, Nat. Phys. **7**, 412 (2011).
[6] H. Miyake, G. A. Siviloglou, C. J. Kennedy, W. C. Burton, and W. Ketterle, Phys. Rev. Lett. **111**, 185302 (2013).
[7] M. Aidelsburger, M. Atala, M. Lohse, J. T. Barreiro, B. Paredes, and I. Bloch, Phys. Rev. Lett. **111**, 185301 (2013).
[8] Y. A. Bychkov and E. I. Rashba, J. Phys. C **17**, 6039 (1984).
[9] G. Dresselhaus, Phys. Rev. **100**, 580 (1955).
[10] A. Manchon, H. C. Koo, J. Nitta, S. M. Frolov, and R. A. Duine, Nat. Mater. **14**, 871 (2015).
[11] Y.-J. Lin, K. Jimenez-Garcia, and I. B. Spielman, Nature (London) **471**, 83 (2011).
[12] N. Q. Burdick, Y. Tang, and B. L. Lev, Phys. Rev. X **6**, 031022 (2016).
[13] I. B. Spielman, P. R. Johnson, J. H. Huckans, C. D. Fertig, S. L. Rolston, W. D. Phillips, and J. V. Porto, Phys. Rev. A **73**, 020702 (2006).
[14] M. A. Khamehchi, C. Qu, M. E. Mossman, C. Zhang, and P. Engels, Nat. Commun. **7**, 10867 (2016), article.
[15] D. Hügel and B. Paredes, Phys. Rev. A **89**, 023619 (2014).
[16] M. Atala, M. Aidelsburger, M. Lohse, J. T. Barreiro, B. Paredes, and I. Bloch, Nat. Phys. **10**, 588 (2014).
[17] T. L. Ho and S. Zhang, Phys. Rev. Lett. **107**, 150403 (2011).
[18] C. Wang, C. Gao, C.-M. Jian, and H. Zhai, Phys. Rev. Lett. **105**, 160403 (2010).
[19] Y. Li, L. P. Pitaevskii, and S. Stringari, Phys. Rev. Lett. **108**, 225301 (2012).
[20] M. Boninsegni and N. V. Prokof'ev, Rev. Mod. Phys. **84**, 759 (2012).
[21] G. I. Martone, Y. Li, and S. Stringari, Phys. Rev. A **90**, 041604 (2014).
[22] More specifically, our scheme realizes 1D SOC in the 2D free space orthogonal to the superlattice.
[23] See Supplemental Material at http://link.aps.org/supplemental/10.1103/PhysRevLett.117.185301 for derivations and experimental details, which includes Ref. [24].
[24] J. Stenger, S. Inouye, A. P. Chikkatur, D. M. Stamper-Kurn, D. E. Pritchard, and W. Ketterle, Phys. Rev. Lett. **82**, 4569 (1999).
[25] An alternative view is that this system is a superposition of two BECs with two spontaneously broken U(1) symmetries (the overall phase, and the relative phase θ). The phase θ determines the orientation of the antiferromagnetic pseudospin texture in the spin x-y plane. The spin texture breaks the lattice symmetry by doubling the lattice constant. This system therefore does not fulfill a stronger definition of supersolidity that demands breaking a continuous translational symmetry.
[26] K. Baumann, C. Guerlin, F. Brennecke, and T. Esslinger, Nature (London) **464**, 1301 (2010).
[27] Y. Chen, J. Ye, and G. Tian, J. Low Temp. Phys. **169**, 149 (2012).
[28] X. Luo, L. Wu, J. Chen, Q. Guan, K. Gao, Z. Xu, L. You, and R. Wang, Sci. Rep. **6**, 18983 (2016).
[29] Collisional losses could be further diminished by reducing the overlap between the pseudospin states. The consequently reduced spin-orbit coupling strength can be compensated by higher intensity Raman beams up to the point where higher order effects and additional heating occur due to nonperturbative driving. The parameters of Fig. 4 were close to this limit.
[30] H. Miyake, G. A. Siviloglou, G. Puentes, D. E. Pritchard, W. Ketterle, and D. M. Weld, Phys. Rev. Lett. **107**, 175302 (2011).
[31] S.-W. Su, S.-C. Gou, Q. Sun, L. Wen, W.-M. Liu, A.-C. Ji, J. Ruseckas, and G. Juzeliūnas, Phys. Rev. A **93**, 053630 (2016).
[32] J. Dalibard, F. Gerbier, G. Juzeliūnas, and P. Öhberg, Rev. Mod. Phys. **83**, 1523 (2011).
[33] K. Osterloh, M. Baig, L. Santos, P. Zoller, and M. Lewenstein, Phys. Rev. Lett. **95**, 010403 (2005).
[34] A. Gorshkov, M. Hermele, V. Gurarie, C. Xu, P. Julienne, J. Ye, P. Zoller, E. Demler, M. Lukin, and A. Rey, Nat. Phys. **6**, 289 (2010).
[35] M. Foss-Feig, M. Hermele, and A. M. Rey, Phys. Rev. A **81**, 051603 (2010).
[36] M. Nakagawa and N. Kawakami, Phys. Rev. Lett. **115**, 165303 (2015).